Available online at www.sciencedirect.com
ScienceDirect
Thin Solid Films 515 (2007) 3171–3178
thin solid films
www.elsevier.com/locate/tsf

Anomalies in stiffness and damping of a 2D discrete viscoelastic system due to negative stiffness components

Yun-Che Wang [a,*], John G. Swadener [a], Roderic S. Lakes [b]

[a] Los Alamos National Laboratory, Los Alamos, New Mexico 87545, USA
[b] Department of Engineering Physics, Engineering Mechanics Program, Biomedical Engineering Department, Materials Science Program and Rheology Research Center, University of Wisconsin-Madison, 147 Engineering Research Building, 1500 Engineering Drive, Madison, WI 53706-1687, USA

Available online 24 February 2006

Abstract

The recent development of using negative stiffness inclusions to achieve extreme overall stiffness and mechanical damping of composite materials reveals a new avenue for constructing high performance materials. One of the negative stiffness sources can be obtained from phase transforming materials in the vicinity of their phase transition, as suggested by the Landau theory. To understand the underlying mechanism from a microscopic viewpoint, we theoretically analyze a 2D, nested triangular lattice cell with pre-chosen elements containing negative stiffness to demonstrate anomalies in overall stiffness and damping. Combining with current knowledge from continuum models, based on the composite theory, such as the Voigt, Reuss, and Hashin–Shtrikman model, we further explore the stability of the system with Lyapunov's indirect stability theorem. The evolution of the microstructure in terms of the discrete system is discussed. A potential application of the results presented here is to develop special thin films with unusual in-plane mechanical properties.

Keywords: Negative stiffness; Viscoelasticity; Lyapunov stability

1. Introduction

For mechanical systems containing a negative stiffness phase, anomalies in stiffness and damping have been observed experimentally [1,2] and described theoretically [3–7]. These references establish the connection between the anomalous phenomena and composite theory, according to the Voigt, Reuss and Hashin–Shtrikman model. Negative stiffness can result from a phase change to lower density in one grain. Significant interactions at the interface between a negative stiffness and positive stiffness phase have been shown to be the cause of the extreme overall stiffness and damping. The interactions can be envisioned as different vibrational modes in the context of dynamics, where the extreme stiffening effect due to the negative stiffness phase resembles that an anti-resonance peak originates from a specific mode that minimizes vibration amplitudes. While the analogy between a vibrational system and the negative stiffness composite system can be established, it should be emphasized that the anomalies due to negative stiffness can occur in the quasi-static limit, i.e. with zero external driving frequency. We remark that the negative Poisson's ratio material, reported in [8,9], should be distinguished from the negative stiffness material in that the former is stable for a Poisson's ratio, ν, in the range $-1<\nu<0$, and the latter is unstable but can be observed experimentally through displacement control. A composite system, consisting of positive and negative stiffness phases, can be stabilized by a surface constraint of the matrix upon the inclusions, provided the matrix is stiff enough. If, however, the negative stiffness inclusions violate strong ellipticity conditions [3], then they are expected to form bands as a result of continuum instability.

Our stability analysis follows the Lyapunov indirect theorem in the dynamical systems theory [10]. Contrary to conventional stability theory based on energy arguments, the Lyapunov theorem investigates stability of a dynamical system. According to the energy-based stability theory, for purely elastic systems in the continuum limit, the Gibbs free energy may be the appropriate potential to investigate the elastic instability under homogeneous deformation when the system is under load

* Corresponding author. Tel.: +1 505 606 0279.
E-mail address: yunche@lanl.gov (Y.-C. Wang).

0040-6090/$ - see front matter © 2006 Elsevier B.V. All rights reserved.
doi:10.1016/j.tsf.2006.01.031

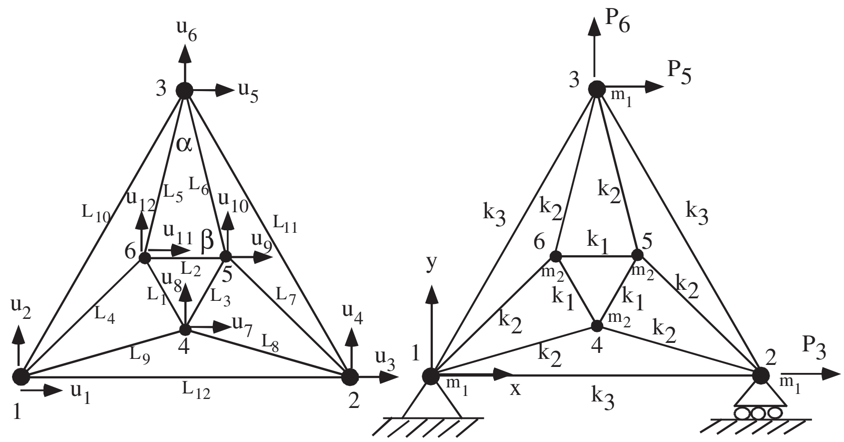

Fig. 1. Configuration of the nested triangular cell composed of 12 two-force members, shown as solid lines. Each element of the inner triangle (Δ456) has stiffness k_1, and each element of the outer triangle (Δ123) has stiffness k_3. The stiffness of linking element between inner and outer triangle is denoted k_2. Solid circles represent mass points: m_1 for the outer and m_2 for the inner. The length of an element of the inner triangle is 5 mm, and the radius of outer triangle is 5.6 times greater than that of the inner. $\alpha = 2\sin^{-1}\left(\frac{L_2}{2L_6}\right)$. $\beta=(\pi-\alpha)/2$. Loading conditions (P_1, P_2, P_3) are so arranged that the lattice cell may experience hydrostatic pressure, simple shear or uniaxial compression.

control [11,12]. However, when some interior points of the material are relatively less stable and remote from the external boundary, the Helmholtz free energy becomes the appropriate potential energy for probing local instability based on the Born and Huang theory [13–15]. This theory can be viewed as an extension of the Lyapunov indirect theorem in the theory of linear elasticity with pre-stress. Furthermore, the Lyapunov method can deal with non-conservative systems, such as a viscoelastic one. Examination of the influence of negative bulk modulus on effective stiffness of a mechanical system in elasticity can be found in Reference [16], where several mechanical systems are analyzed for their stability along the direction of applied force.

Thin films are the manifestation of two-dimensional materials. The purpose of this paper is to demonstrate and analyze anomalous mechanical properties, structural evolution and stability of a two dimensional discrete structure due to negative stiffness effects under in-plane loading. This structure can be realized as a cell or building block for a lattice. The lattice will be stable if all the cells in it are stable. For thin films, the lattice would represent a pattern of negative stiffness and positive stiffness phases. The repeat unit in the pattern would be represented by a cell. Special attention is placed on the structural integrity and stability of the system when it exhibits extreme mechanical properties, such as stiffness and damping.

In our analysis, geometrical linearity is assumed; however, the use of negative stiffness for an element implies the consideration of geometric nonlinearity on that element [4]. That is to say that the negative stiffness in the element is a result of its deformed geometry, which is taken as the initial reference position for the equilibrium analysis. The analysis from this point forward assumes geometric linearity. Each element of the system is assumed to be a standard linear solid with selected elements containing negative stiffness. The limitations of linear models reflecting limited reality are acknowledged. However, through the linear analysis, we can obtain further understandings of the system with a negative stiffness inclusion, as the following: (1) structure evolution corresponding to quasi-static processes, (2) damping with respect to different deformation modes and (3) stability of the extreme properties.

2. Analysis

A nested triangular lattice cell, as shown in Fig. 1, is of interest to explore stable extreme mechanical properties. The figure shows the node numbers, load and displacement boundary conditions, and displacement coordinates at each node. The elements adopted here are the two-force members, also known as the truss element in structural mechanics, depicted as the solid lines connecting the solid circles in the figure. Fig. 2 shows a single element, used in our analysis, in its local and global coordinates. In the triangular cell, there are 12 elements that enclose 7 single domain triangles. In the following, we formulate the mechanical problem of the triangular lattice cell, based on the

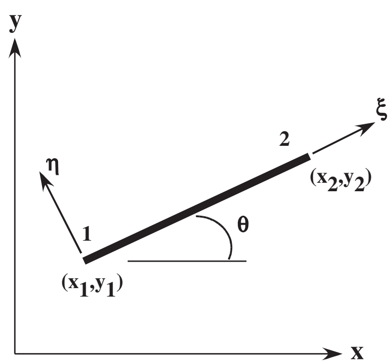

Fig. 2. A schematic for a two-dimensional spring element in its local (ξ–η) and global (x–y) coordinate system.

12 elements and 6 nodes, into a mathematical form with the spirit of the finite element method. One can solve other lattice geometry by simply redefining nodes, elements and connectivity conditions between nodes and elements.

The inner (k_1) and outer triangle (k_3) are equilateral, i.e. $L_1=L_2=L_3$, and $L_{10}=L_{11}=L_{12}$. Each of the links between the inner and outer triangle has the spring constant k_2. A symmetry assumption is applied in the material properties of the elements, in accordance with the symmetry of the geometry. We assume that only k_1 can have negative stiffness. It is noted that to fully maintain the symmetry, the loading, P_3, P_5 and P_6 cannot be totally arbitrary. To test the bulk stiffness of the model by analogously applying hydrostatic pressure on the lattice cell, we assume $P_3=-\gamma\cos(\pi/6)$, $P_5=0$ and $P_6=-\gamma$. As for a simple shear test, we set $P_3=-\gamma$, $P_5=\gamma$ and $P_6=0$; a uniaxial compression simulation, $P_3=0$, $P_5=0$ and $P_6=-\gamma$. It can be verified that all the forces, applied loads and reaction forces from the supports, point at the center of the structure for the bulk mode. To calculate the mechanical responses of the structure, the finite element method [17] is adopted. For a purely elastic analysis, the elements are structural trusses. The elemental stiffness matrix of a truss can be written as follows, with the definition of θ shown in Fig. 2.

$$\mathbf{k}=k\begin{bmatrix}\cos^2\theta & \cos\theta\sin\theta & -\cos^2\theta & -\cos\theta\sin\theta\\ \cos\theta\sin\theta & \sin^2\theta & -\cos\theta\sin\theta & -\cos^2\theta\\ -\cos^2\theta & -\cos\theta\sin\theta & \cos^2\theta & \cos\theta\sin\theta\\ -\cos\theta\sin\theta & -\sin^2\theta & \cos\theta\sin\theta & \sin^2\theta\end{bmatrix}. \quad (1)$$

Here k is the stiffness matrix with the dimension of 1 by 1 in the local (ξ–η) coordinate system, and $\mathbf{k}$ the stiffness matrix in the global (x–y) coordinate system. Our method of computation follows the spirit of the finite element method [17], but the equations of motion are expressed in terms of the system's state-space variables, which are displacements, velocities and internal forces. The merit of using this formulation is the ease of incorporating viscoelastic effects and stability analysis. In the finite element method, suitable displacement boundary conditions are necessary to ensure the stiffness matrix of the system is non-singular. The imposed displacement boundary conditions will not limit our exploration about the effects of negative stiffness, but only introduce a rigid-body shift. The equations of motion of the structure in terms of nodal displacements are

$$\mathbf{M}\cdot\ddot{\mathbf{U}}+\mathbf{F}=\mathbf{P}, \quad (2)$$

$$\mathbf{F}=\mathbf{\Lambda}^T\cdot\mathbf{f},\ \text{and} \quad (3)$$

$$f_j+T_{\varepsilon j}\dot{f}_j=k_j(\Delta_j+T_{\sigma j}\dot{\Delta}_j),\ j=1,2,3,...,12, \quad (4)$$

where $\mathbf{M}=\text{diag}[m_2\ m_2\ m_2\ m_1\ m_1\ m_1\ m_1\ m_1\ m_1]\in\Re^{9\times 9}$ is the mass matrix, $\mathbf{U}=[u_3\ u_5\ u_6\ u_7\ u_8\ u_9\ u_{10}\ u_{11}\ u_{12}]^T\in\Re^{9\times 1}$ the displacement vector, $\mathbf{F}$ internal force vector, projected on the global coordinate, and $\mathbf{P}$ the external force vector as indicated in Fig. 1. The operator diag forms a diagonal matrix. The internal force inside each spring element can be collected to form the column vector, as follows.

$$\mathbf{f}=[f_1\ f_2\ f_3\ f_4\ f_5\ f_6\ f_7\ f_8\ f_9\ f_{10}\ f_{11}\ f_{12}]^T\in\Re^{12\times 1}. \quad (5)$$

Essentially, Eq. (4) stipulates that each of the elements in the system behaves as a standard linear solid in the context of linear viscoelasticity. To convert information in the local coordinates ($\xi-\eta$) to the global (x–y) coordinates, we define the contribution matrix, $\mathbf{\Lambda}$, as follows.

$$\mathbf{\Lambda}=\begin{bmatrix}0&0&0&-c_1&-s_1&0&0&c_1&s_1\\ 0&0&0&0&0&c_2&s_2&-c_2&-s_2\\ 0&0&0&-c_3&-s_3&c_3&s_3&0&0\\ 0&0&0&0&0&0&0&c_4&s_4\\ 0&c_5&s_5&0&0&0&0&-c_5&-s_5\\ 0&c_6&s_6&0&0&-c_6&-s_6&0&0\\ c_7&0&0&0&0&-c_7&-s_7&0&0\\ c_8&0&0&-c_8&-s_8&0&0&0&0\\ 0&0&0&-c_9&-s_9&0&0&0&0\\ 0&c_{10}&s_{10}&0&0&0&0&0&0\\ c_{11}&-c_{11}&-s_{11}&0&0&0&0&0&0\\ -c_{12}&0&0&0&0&0&0&0&0\end{bmatrix}. \quad (6)$$

Here c_j and s_j are the direction cosine and sine for the element j. The dimension of $\mathbf{\Lambda}$ is $\Re^{12\times 9}$. The state-space representation of Eqs. (2)–(4) is as follows.

$$\mathbf{A}\cdot\dot{\mathbf{X}}=\mathbf{B}\cdot\mathbf{X}+\mathbf{C} \quad (7)$$

$$\mathbf{A}=\begin{bmatrix}\mathbf{I}_9&\mathbf{0}&\mathbf{0}\\ \mathbf{0}&\mathbf{M}&\mathbf{0}\\ \mathbf{0}&\mathbf{0}&\mathbf{T}_\varepsilon\end{bmatrix}, \quad (8)$$

$$\mathbf{B}=\begin{bmatrix}\mathbf{0}&\mathbf{I}_9&\mathbf{0}\\ \mathbf{0}&\mathbf{0}&-\Lambda^T\\ \mathbf{k}_{\text{ele}}\cdot\mathbf{\Lambda}&\mathbf{k}_{\text{ele}}\cdot\mathbf{T}_\sigma\cdot\mathbf{\Lambda}&-\mathbf{I}_{12}\end{bmatrix}, \quad (9)$$

$$\mathbf{C}=[\mathbf{0}\ \mathbf{P}^T\ \mathbf{0}]^T, \quad (10)$$

$$\mathbf{k}_{\text{ele}}=\text{diag}[k_1\ k_1\ k_1\ k_2\ k_2\ k_2\ k_2\ k_2\ k_2\ k_3\ k_3\ k_3], \quad (11)$$

$$\mathbf{T}_\sigma=\text{diag}[T_{\sigma 1}\ T_{\sigma 1}\ T_{\sigma 1}\ T_{\sigma 2}\ T_{\sigma 2}\ T_{\sigma 2}\ T_{\sigma 2}\ T_{\sigma 2}\ T_{\sigma 2}\ T_{\sigma 3}\ T_{\sigma 3}\ T_{\sigma 3}], \quad (12)$$

$$\mathbf{T}_\varepsilon=\text{diag}[T_{\varepsilon 1}\ T_{\varepsilon 1}\ T_{\varepsilon 1}\ T_{\varepsilon 2}\ T_{\varepsilon 2}\ T_{\varepsilon 2}\ T_{\varepsilon 2}\ T_{\varepsilon 2}\ T_{\varepsilon 2}\ T_{\varepsilon 3}\ T_{\varepsilon 3}\ T_{\varepsilon 3}], \quad (13)$$

where $\mathbf{V}=[\dot{u}_3\ \dot{u}_5\ \dot{u}_6\ \dot{u}_7\ \dot{u}_8\ \dot{u}_9\ \dot{u}_{10}\ \dot{u}_{11}\ \dot{u}_{12}]^T\in\Re^{9\times 1}$ is the velocity vector, and $\mathbf{X}=[\mathbf{U}\ \mathbf{V}\ \mathbf{f}]^T\in\Re^{30\times 1}$ the state-space vector of the system. The subscript of the symbol **I** indicates the dimension of the identity matrix **I**. $\mathbf{k}_{\mathrm{ele}}$ presents the stiffness matrix in the local coordinate system. $\mathbf{T}_\sigma$ and $\mathbf{T}_\varepsilon$ are matrices containing the time constants for each element. We remark that one can use the consistent mass matrix, calculated by $\mathbf{\Lambda}^T \bullet \mathbf{M}' \bullet \mathbf{\Lambda}$, where

$$\mathbf{M}' = \mathrm{diag}\,[m_2\ m_2\ m_2\ m_2\ m_2\ m_2\ m_1\ m_1\ m_1\ m_1\ m_1\ m_1] \in \Re^{12\times 12}, \tag{14}$$

to obtain more accurate solutions. However, with the purpose of observing the anomalies in stiffness and damping in the low frequency regime, we use the lumped mass matrix and set $m_j = 10^{-12}$ kg, where $j = 1, 2$, denoting the mass points at the corners of the inner and outer triangle, respectively, to diminish inertia effects and increase natural resonant frequencies of the structure so large that the difference between the use of the diagonal or consistent mass matrix becomes indistinguishable. The required computational time to invert a diagonal mass matrix is minimal, compared to the consistent mass matrix. Since the mass matrix does not come into play in static analysis, the concern, if any, with the influence of the mass matrix comes when one tries to analyze the stability and dynamical behavior of the system.

To calculate the damping properties of the system in terms of the loss tangent, we take a Fourier transformation on the governing equations, Eqs. (2)–(4), for obtaining the dynamic stiffness of the system in the frequency domain, as follows.

$$\mathbf{K}^* = -\omega^2 \mathbf{M} + \mathbf{\Lambda}^T \bullet (\mathbf{I}_{12} + i\omega \mathbf{T}_\varepsilon)^{-1} \bullet (\mathbf{k}_{\mathrm{ele}} \mathbf{\Lambda} + i\omega \mathbf{k}_{\mathrm{ele}} \mathbf{T}_\sigma \mathbf{\Lambda}). \tag{15}$$

By the generalization of the definition of the loss tangent for a 1-d.o.f. system, the effective loss tangent of the system can be calculated as follows.

$$\tan\delta_j = \mathrm{Im}(\zeta_j)/\mathrm{Re}(\zeta_j),\ j = 1, 2, ..., 9. \tag{16}$$

where ζ_j is the eigenvalue of $\mathbf{K}^*$ corresponding the degree of freedom along P_j. In other words, there are 9 tan δ's associated with the discrete system, corresponding to the 9 d.o.f. system. It is noted that each of the loss tangent components corresponds to the phase lag information of a specific load-deformation mode. We remark that although the above formulation is based on the triangular lattice element, as shown in Fig. 1, with 9 degrees of freedom, following the same framework, it is straightforward to solve the system with different geometry.

Following Lyapunov's indirect stability theorem, our stability analysis requires the calculation of the eigenvalues of the matrix $\mathbf{A}^{-1}\mathbf{B}$ from Eq. (7). The number of eigenvalues is equal to $2*(2*n-3)+2*n$, where n is the number of nodes. Specifically, for the triangular cell, $n=6$, and thus the total number of eigenvalues is 30. This number may well exceed one's expectation from experience with Hamiltonian system since our system is non-Hamiltonian, and the mathematical formulation is based on the state-space representation.

In three-dimensional continuum theory, according to Born and Huang [13], we remark that the internal stability of the material body can be studied by analyzing the sign of the eigenvalue λ in the following equation.

$$(C_{pqrs} k_q k_s - \rho \lambda^2 \delta_{pr}) \tilde{u}_r = \tilde{b}_p. \tag{17}$$

Here for isotropic materials $C_{pqrs} = \lambda \varepsilon_{rs} \delta_{pq} \delta_{rs} + \mu(\varepsilon_{pq} + \varepsilon_{qp})$. The symbol k_j denotes the wave vector along the j direction in three dimensions and ρ the density of the material; $\tilde{u}_j$ and $\tilde{b}_j$ are displacement and body force, respectively, in the Fourier space. The material body is internal unstable if the imaginary part of λ is less than zero. The stability conditions of all crystal classes have been summarized in Reference [18].

3. Results and discussion

For the triangular lattice cell, Fig. 3 shows the result of the overall bulk stiffness and normalized change of area, $(A_f - A_0)/A_0$, versus the tuning parameter k_1, under the quasi-static assumption ($\omega = 0$ rad/s). Throughout the analysis, $k_2 = 5$ and $k_3 = 10$ kN/m. Fixing these two parameters will not lose the generality of our analysis since only the relative relationship of k_1, k_2 and k_3 is important in the search of the anomalies. As expected, the measured change of area is strongly related to that of overall stiffness. Here A_0 is the original area of the outer or inner triangle shown in Fig. 1, and A_f is the area of the corresponding triangle after deformation. The bulk stiffness is defined as P_6/u_6, the ratio of the vertical load to vertical displacement at node 3. It can be seen that the system shares the same feature as the 1-D system, reported in [4], i.e. its overall

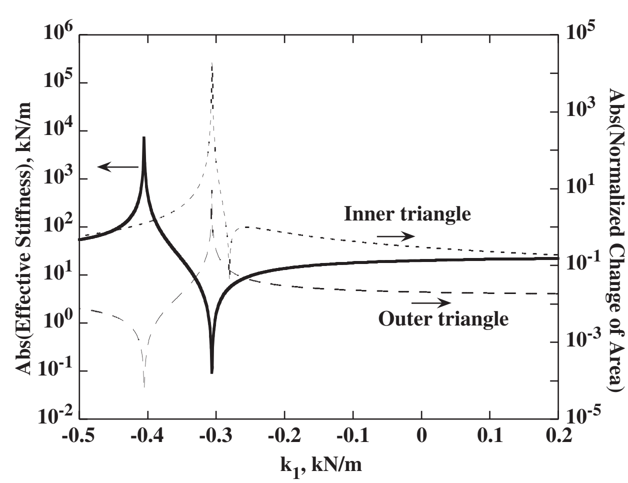

Fig. 3. Overall stiffness, measured at node 3 along y-direction, i.e. P_6/u_6, and change of structural shape $(A_f/A_0 - 1)$ versus the tuning parameter k_1. All elements are elastic, and the quasi-static process is assumed. Extreme overall stiffness is observed at $k_1 = -0.4$ kN/m, corresponding to minimal area change on the outer triangle. The dip appears around $k_1 = -0.27$ kN/m on the curve of normalized change of inner triangle area is due to the re-orientation of the inner triangle, which can be observed in Fig. 4.

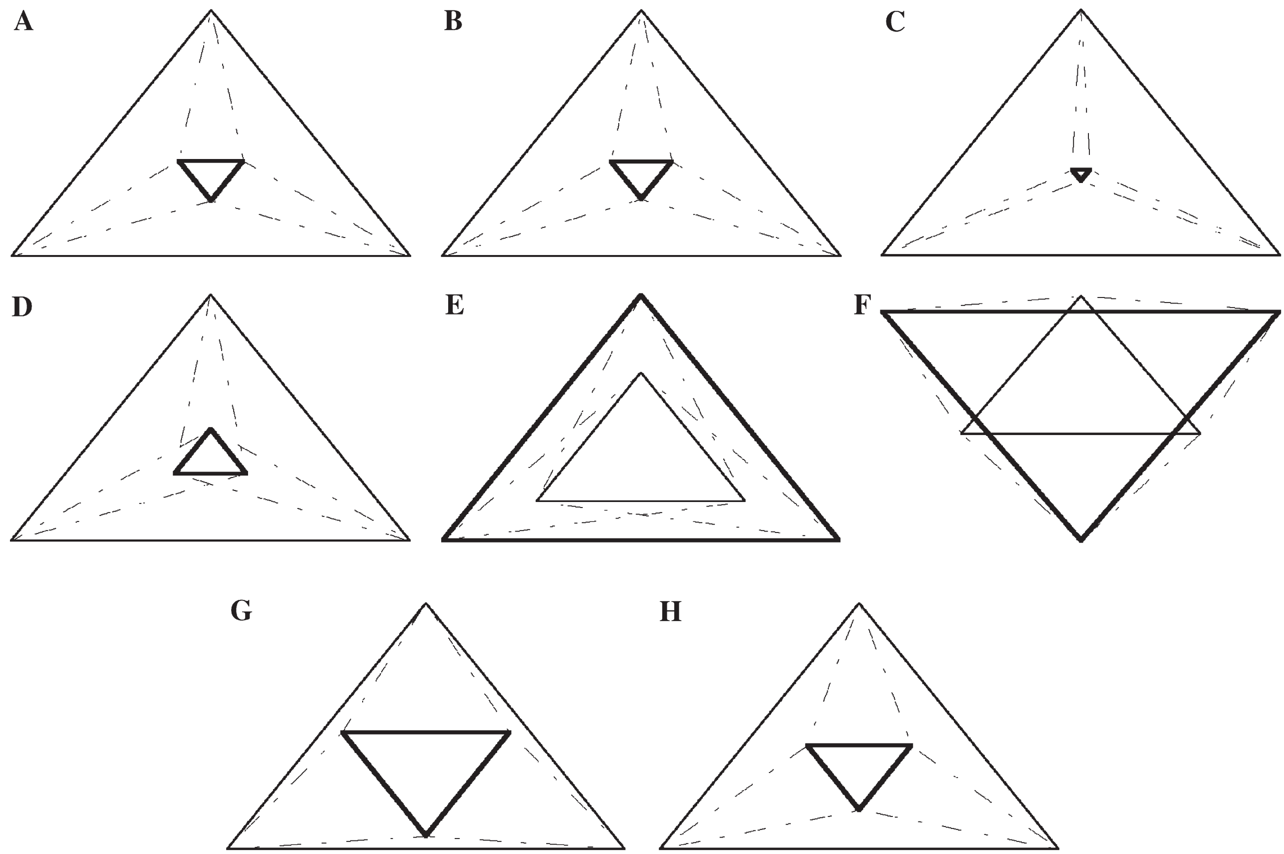

Fig. 4. Deformation under hydrostatic compression. (A) $k_1 = 0.2$, (B) $k_1 = 0$, (C) $k_1 = -0.25$, (D) $k_1 = -0.29$, (E) $k_1 = -0.3$, (F) $k_1 = -0.32$, (G) $k_1 = -0.35$ and (H) $k_1 = -0.4$. The stiffness is in units of kN/m. The graphs are normalized to the outer boundary. The steps for the evolution of the inner triangle are first size reduction, then reverse, expansion, reverse again, and finally decrease in size to a size-invariant state.

bulk stiffness reaching a minimum first and then a maximum while decreasing k_1. We remark that due to the symmetry of geometry, material properties and the loading condition, P_6/u_6 represents the bulk property of the structure. The unsymmetrical displacement boundary conditions cause the structure not to deform in a completely symmetrical way. However, this effect is negligible.

Comparing the normalized area change of the inner and outer triangle with the stiffness of the system, one can see that significant anomalies in structural shape occur in both the inner and outer triangle when the stiffness of the system reaches its minimum. More interestingly, the normalized change of inner triangular area reaches a minimum at $k_1 \sim -2.7$ kN/m before its maximum at $k_1 \sim -0.3$ kN/m. This is due to the re-orientation of the inner triangle. With sufficient degrees of numerical resolution, the magnitude of the dip at $k_1 \sim -2.7$ kN/m would be zero, indicating the deformed area is the same as the undeformed one. Although the two areas are identical, they exhibit different orientations, as shown in Fig. 4 (B) and (D). However, it can be seen that change of the orientation of the inner triangle does not significantly influence the overall stiffness. Moreover, the size of the inner triangle shrinks to zero before changing its orientation. For the configuration with extreme high stiffness ($k_1 = -0.4$ kN/m), there is not much change in the inner triangle in size, but the change of the outer triangle reaches a minimum, corresponding highest stiffness.

The evolution of the nested triangular structure is shown in Fig. 4, as k_1 decreases from positive to negative. Each figure is

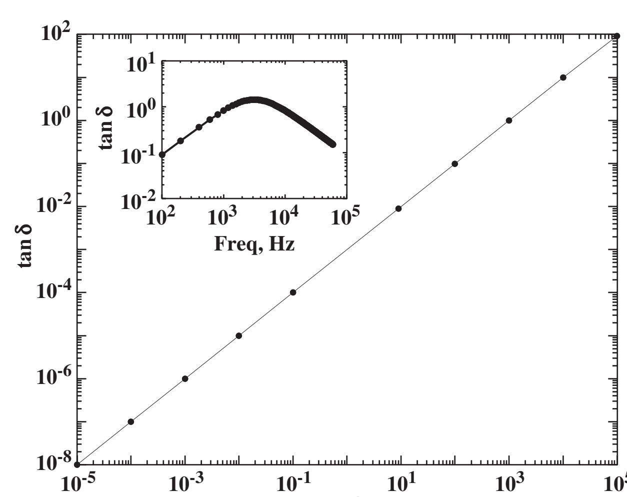

Fig. 5. Relationship between tan δ and r for the standard linear solid in the context of viscoelasticity with $\omega = 10$ rad/s and $\tau_\varepsilon = 10^{-4}$ s. The inset shows the Debye peak in the frequency domain for the standard linear solid with $r = 10$ and $\tau_\varepsilon = 10^{-4}$ s.

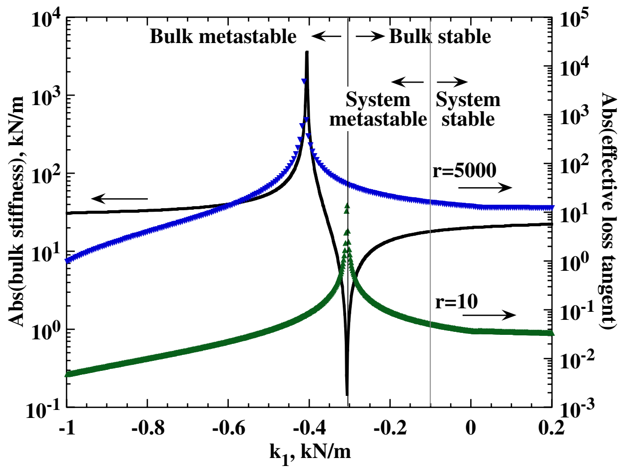

Fig. 6. Bulk stiffness and effective loss tangent versus k_1. The bulk stiffness is measured by P_6/u_6. $r=\tau_{\sigma j}/\tau_{\varepsilon j}$, for $j=1,2,3$. $\omega=10$ rad/s. Note that the damping peak moves toward the extreme stiffness state as r increases. Bulk stability is defined when the eigenvalue corresponding the bulk mode contains positive real part. System instability is occurred when a stability losing eigenvalue is observed with the smallest k_1 in magnitude. Detailed eigenvalue analysis is shown in Fig. 9. The system instability is due to a shear mode. High damping and high stiffness can be obtained simultaneously around $k_1=-0.4$ kN/m, but in the meta-stable regime.

normalized to the outermost boundary. During the process of decreasing k_1, we observe that first from (A) to (C) the size of the inner triangle decreases with k_1, until a minimum (zero size), and then a change of orientation follows, as shown in (D). When k_1 continues decreasing, the size of the inner triangle increases abruptly, approaching the size of the outer triangle, as shown in (E). After that, another change of orientation follows, and then the size of inner triangle decreases as k_1 decreases, as shown in (F) and (G). Finally, in (H), the size of the triangles are insensitive to k_1. Compared with the stiffness evolution of the system with respect to k_1 in Fig. 3, the configuration corresponding to the highest stiffness is similar to Fig. 4 (H).

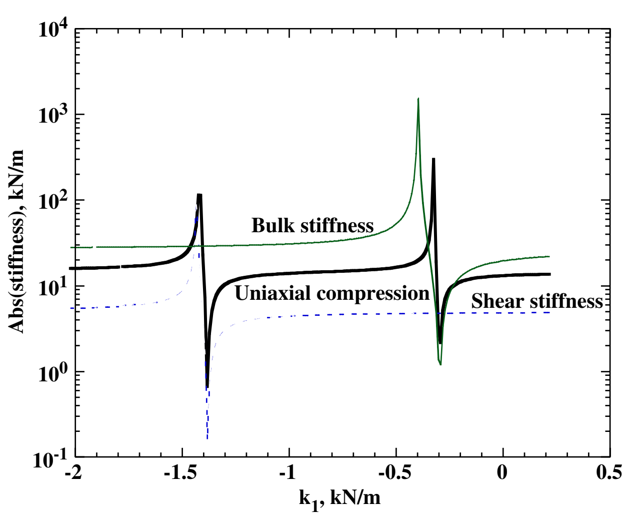

Fig. 7. Effective stiffness of the triangular lattice cell with respect to different loading modes. Since the process is quasi-static, the effective stiffness is independent of the viscoelastic parameter r. Bulk or compression stiffness is measured by P_6/u_6. Shear stiffness is measured by P_5/u_5.

Physically, this evolution demonstrates the significant interaction between the positive-stiffness and negative-stiffness phases.

As for the damping and stability calculations, viscoelastic time constants of elements and driving frequency are important. We choose $\tau_{\varepsilon 1}=10^{-4}$, $\tau_{\varepsilon 2}=5\times 10^{-4}$ and $\tau_{\varepsilon 3}=2\times 10^{-4}$ seconds, and $\tau_{\sigma j}=r_j\,\tau_{\varepsilon j}$, where $j=1, 2, 3$, for the inner triangle, links and outer triangle, respectively. And, we set the driving frequency $\omega=10$ rad/s throughout. The physical meaning of the dimensionless parameter r relates to the strength of viscoelasticity [19]. More commonly, the loss tangent, $\tan\delta_j$, for the element j is adopted to describe the linear viscoelastic properties of material. For a standard linear solid, the relationship between r_j and $\tan\delta_j$ is $\tan\delta_j=\omega(r_j-1)\tau_{\varepsilon j}/(1+r_j\omega^2\tau_{\varepsilon j}^2)$ for the element j. Fig. 5 shows the relationship between $\tan\delta$ and r for the standard linear solid with $\omega=10$ rad/s and $\tau_{\varepsilon j}=10^{-4}$ s. The inset of Fig. 5 demonstrates the Debye peak of the standard linear solid in the frequency domain with the assumptions of $r_j=10$ and $\tau_{\varepsilon j}=10^{-4}$ s. To simplify our analysis in the parameter space of r_j, we assume $r_1=r_2=r_3=r$. Furthermore, since our interest is in demonstrating the anomalies in the low frequency regime, we set the driving frequency ω to be 10 rad/s throughout, and use the dimensionless parameter r to measure the strength of viscoelasticity in the elements of the system.

As r increases, the baseline $\tan\delta$ for the system increases, as shown in Fig. 6, while under hydrostatic loading. Although the quasi-static effective stiffness of the system is independent of the

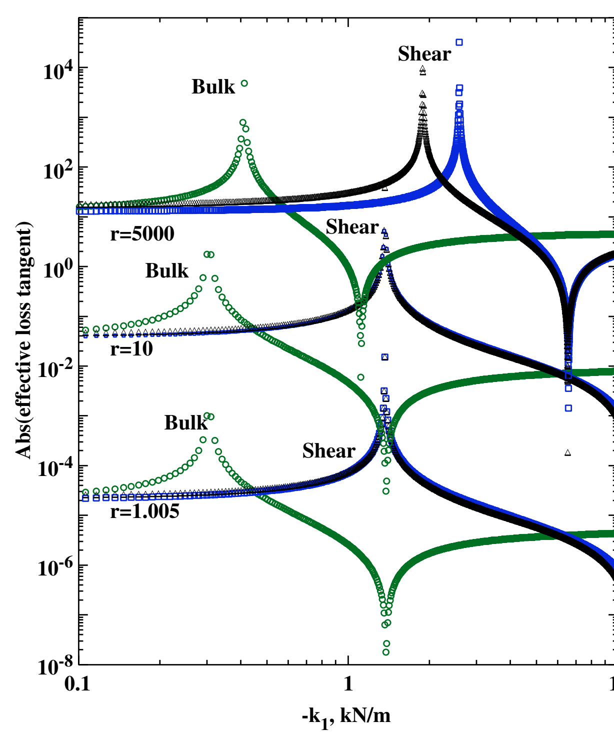

Fig. 8. Loss tangent of the triangular lattice cell with various r versus $-k_1$. Driving frequency (ω) is 10 rad/s. Modes with anomalous peaks are shown. The curves labeled with open circles are due to bulk responses, and those with triangles and open squares are due to shear modes. Anomalous peaks are found around $k_1=-0.3$ kN/m for the bulk responses, and around $k_1=-1.4$ kN/m the shear mode. A peak split in the shear response with $r=5000$ is observed. The magnitude of r is associated with the baseline damping of the modes.

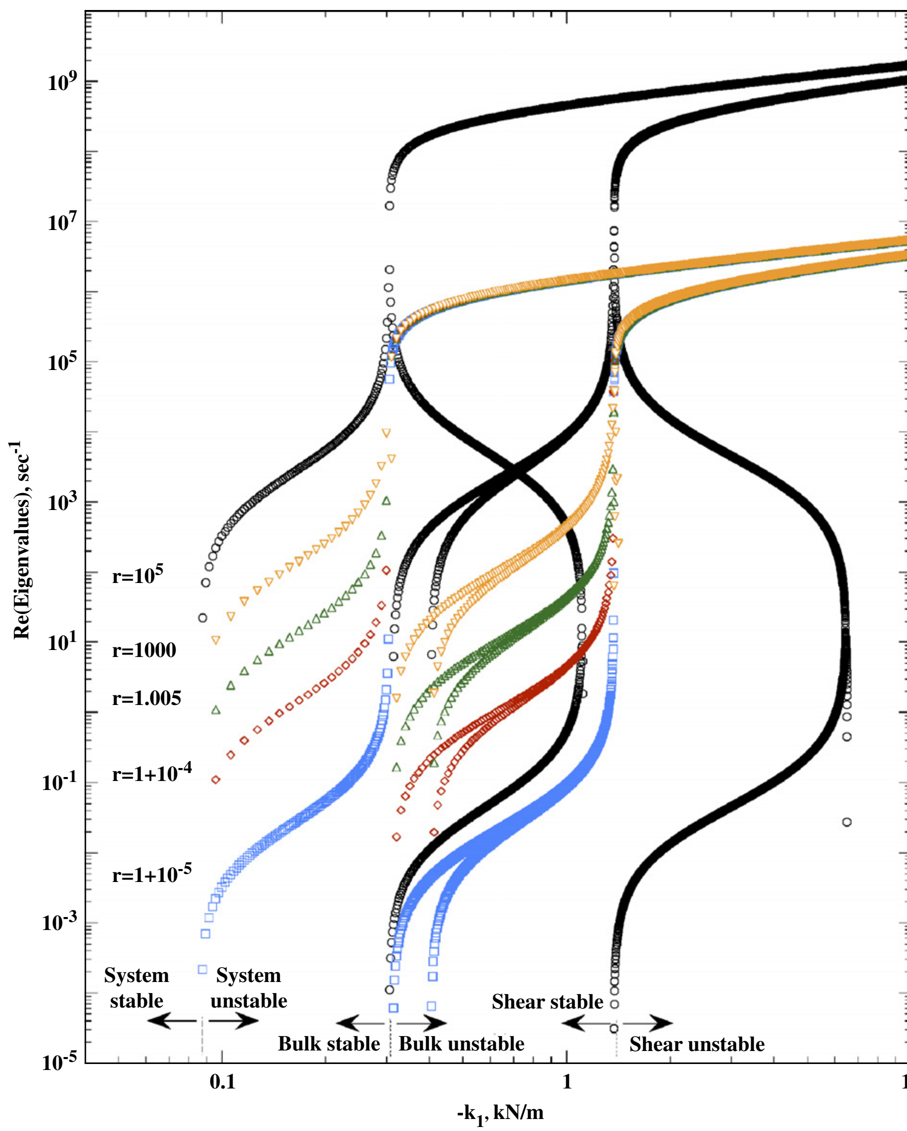

Fig. 9. Stability analysis with various r for $m_1 = m_2 = 10^{-12}$ kg. The stability losing eigenvalues at $k_1 = -0.9$ kN/m dominates the stability of the system. The eigenvalues corresponding different loading modes are labeled. Each symbol with an assigned r value indicates the trend of stability losing eigenvalues with respect to the tuning parameter $-k_1$. For each r, the curves vanish at their lower ends, providing the information of losing stability. For example, the open-square curves end at $k_1 = -0.09$, -0.3, and -0.4 kN/m, and stability is identified by recognizing on the left hand side of the curves at these values the real part of eigenvalues is negative, indicating stability, and on the right hand side the eigenvalues contain positive real parts, signature of instability. The magnitude of the eigenvalues increases with r, demonstrating the characteristic of meta-stability.

parameter r, overall tan δ, calculated by Eq. (16), strongly depends on r. It can be seen that for $r = 10$, the system exhibits high compliance and high damping simultaneously, and when r is about 5000, high stiffness and high damping can be achieved at the same time, albeit in the meta-stable domain. For high damping and high stiffness applications, the parameter set, $k_1 = -0.4$, $k_2 = 5$, $k_3 = 10$ kN/m and $r = 5000$, appears to be feasible, although its lifetime may be short. It is understood that the meta-stability originates from the finite time constant (i.e. the inverse of the eigenvalues) associated with divergence of deformation responses [7]. Furthermore, in Fig. 6, we observe the structure exhibits a system instability before the instability due to the bulk mode. An asymmetric shear mode may be responsible for the system instability.

Results of our tan δ analysis for the structure are shown in Fig. 8; multiple peaks are observed. Comparing with effective stiffness under different loading conditions, as shown in Fig. 7, we identify that different damping peaks correspond to different loading cases. The damping peak around $k_1 = -0.3$ kN/m is accompanied by the stiffness anomaly, calculated under hydrostatic loading. Under simple shear, the system exhibits stiffness and damping anomaly around $k_1 = -1.5$ kN/m. In the case of uni-axial compression, we observe two anomalies in the system's effective stiffness; one coincides with the bulk mode response and the other the shear mode. A peak split is observed with $r = 5000$ for the shear mode. We note that although for the case $r = 1.005$, the damping anti-peak of the bulk mode appears at about the same k_1 as the damping peak of the shear mode, one can take advantage of either damping peak by exciting its corresponding mode.

By increasing the stiffness of the linking springs (i.e. k_2 springs), it is also observed (not shown) that in order to obtain the extreme stiffness peak, it requires k_1 to be more negative. Therefore, it becomes experimentally unrealizable with larger k_2 due to high degrees of instability. Physically, this result is consistent with the prediction from continuum theory in that if k_2 approaches infinity, the system becomes system with negative stiffness elements under load control, and it is unstable.

We remark that only one of the 9 tan δ's from Eq. (16) represents physical overall loss tangent of the system under a certain deformation mode. And, it is possible to identify modes without completely analyzing eigenvectors of the system since the physically relevant tan δ can be singled out by recognizing that the maximal compliance is in close relation to the maximal damping during the negative-stiffness tuning process. Comparison of different modes for the triangular lattice cell is shown in Figs. 7 and 8 for the effective stiffness and tan δ. It can be realized that each of the damping peaks corresponds to a specific deformation mode. For example, the damping peak at $k_1 = -0.3$ kN/m is associated with the bulk mode, and that at $k_1 = -1.5$ kN/m corresponds to the shear mode. This result is consistent with the 1-D system containing negative stiffness [5], and one expects that extreme stiffness accompanies extreme damping. Furthermore, we remark that since it requires more negative k_1 to obtain high stiffness in the shear mode, the stability of the shear mode is weaker that that of the bulk mode.

Fig. 9 shows the results of our eigenvalue analysis with k_1 as a tuning parameter for $m_1 = m_2 = 10^{-12}$ kg, The degree of instability can be related to the magnitude of the stability losing eigenvalues. Note that, in order to plot the x-axis on the log scale, we use $-k_1$ as the horizontal axis, and the eigenvalues are in units of 1/s. Instability occurs when the real parts of eigenvalues become positive. The loss of stability is determined by the disappearance of the curves at their lower ends. Fig. 9 indicates the structure of eigenvalue curves does not change significantly with different strength of viscoelasticity. We remark that at the zero mass limit, the degree of instability is lesser as the strength of viscoelasticity in the elements increases, and stability of the structure depends on the corresponding deformation modes. However, slight perturbation will excite the stability losing eigenvalues at $k_1 = -0.9$ kN/m, causing system instability.

Although at a certain transition the change of structure geometry is enormous in order to maintain the force equilibrium between the positive-stiffness and negative-stiffness elements, it appears that, around the point that the system exhibits extreme high stiffness, the structure geometry is regular. Our analysis demonstrates firstly that a structure can be completely stable even when negative stiffness elements are present, such as when $-0.9 < k_1 < 0$ kN/m for the present case. Secondly, with negative stiffness elements, the stable and meta-stable anomalies of the system can be obtained.

Thin films with anomalous material properties may be envisaged in light of the present research. Controlled phase transformations of materials can give rise to negative stiffness via the gradient of the energy curve in the Landau theory. We claim that the heterogeneity required to achieve a balance between positive and negative stiffness phases might be obtainable using microlithography or nanolithography, as described in [20]. Alternatively, one can manufacture a film containing nano-grain inclusions of phase transforming material, such as VO_2, through sputtering deposition [21] or pulsed laser deposition [22].

4. Conclusions

We conclude that the two-dimensional systems with negative stiffness have essentially features as the one-dimensional systems. In other words, one can obtain stable extreme damping and meta-stable extreme stiffness in two dimensions. However, slight perturbations may excite other modes in the system, which make the 2D system appear to have weaker stability. The reduction in stability due to coupling between modes may depend on the geometrical configuration of the system.

Acknowledgement

This research is funded by DOE, Office of Science, Office of Basic Energy Science. Y.-C. W. acknowledges support from LANL director's funded post-doctoral fellowship. R.S.L. is grateful for a grant, CMS-0136986, from NSF.

References

[1] R.S. Lakes, Philos. Mag. Lett. 81 (2001) 95.
[2] R.S. Lakes, T. Lee, A. Bersie, Y.C. Wang, Nature 410 (2001) 565.
[3] R.S. Lakes, J.W. Drugan, J. Mech. Phys. Solids 50 (2002) 979.
[4] Y.C. Wang, R.S. Lakes, Am. J. Phys. 72 (2004) 40.
[5] Y.C. Wang, R.S. Lakes, Appl. Phys. Lett. 84 (2004) 4451.
[6] Y.C. Wang, R.S. Lakes, Q. Appl. Math. 63 (2005) 34.
[7] Y.C. Wang, R.S. Lakes, Philos. Mag. 84 (2004) 3785.
[8] R.S. Lakes, Science 235 (1987) 1038.
[9] R.S. Lakes, Adv. Mater. (Weinheim, Germany) 5 (1993) 293.
[10] S.H. Strogatz, Nonlinear Dynamics and Chaos, Perseus Books, Cambridge, Massachusetts, 1994.
[11] D.C. Wallace, Thermodynamics of Crystals, Wiley, New York, 1972.
[12] J.W. Morris Jr., C.R. Krenn, Philos. Mag., A 80 (2000) 2827.
[13] M. Born, K. Huang, Dynamical Theory of Crystal Lattices, Oxford, UK, 1954.
[14] J. Li, K.J. Van Vliet, T. Zhu, S. Yip, S. Suresh, Nature 418 (2002) 307.
[15] K.J. Van Vliet, J. Li, T. Zhu, S. Yip, S. Suresh, Phys. Rev., B 67 (2003) 104105.
[16] Y.C. Wang, R.S. Lakes, J. Compos. Mater. 39 (2005) 1645.
[17] R.D. Cook, D.S. Malkus, M.E. Plesha, Concepts and Applications of Finite Element Analysis, 3rd edition, John Wiley and Sons, New York, 1989.
[18] R.A. Cowley, Phys. Rev., B 13 (1976) 4877.
[19] C. Zener, Elasticity and Anelasticity of Metals, The University of Chicago Press, Illinois, Chicago, 1948.
[20] H.G. Craighead, Science 290 (2000) 1532.
[21] F.Y. Gan, P. Laou, J. Vac. Sci. Technol., A 22 (2004) 879.
[22] J.Y. Suh, R. Lopez, L.C. Feldman, R.F. Haglund Jr., J. Appl. Phys. 96 (2004) 1209.